doi:10.1016/j.jmb.2010.03.039 J. Mol. Biol. (2010) 398, 542–554

JMB

Available online at www.sciencedirect.com

ScienceDirect

ELSEVIER

Mapping of Drebrin Binding Site on F-Actin

Elena E. Grintsevich[1], Vitold E. Galkin[2]†, Albina Orlova[2]†, A. Jimmy Ytterberg[1]†, Mouna M. Mikati[1], Dmitri S. Kudryashov[1], Joseph A. Loo[1,3,4], Edward H. Egelman[2] and Emil Reisler[1,4]*

[1]*Department of Chemistry and Biochemistry, University of California, Los Angeles, CA 90095, USA*

[2]*Department of Biochemistry and Molecular Genetics, University of Virginia, Charlottesville, VA 22908, USA*

[3]*Molecular Biology Institute, University of California, Los Angeles, CA 90095, USA*

[4]*Department of Biological Chemistry, University of California, Los Angeles, CA 90095, USA*

Received 19 November 2009; received in revised form 18 March 2010; accepted 19 March 2010
Available online 27 March 2010

Edited by R. Craig

Drebrin is a filament-binding protein involved in organizing the dendritic pool of actin. Previous *in vivo* studies identified the actin-binding domain of drebrin (DrABD), which causes the same rearrangements in the cytoskeleton as the full-length protein. Site-directed mutagenesis, electron microscopic reconstruction, and chemical cross-linking combined with mass spectrometry analysis were employed here to map the DrABD binding interface on actin filaments. DrABD could be simultaneously attached to two adjacent actin protomers using the combination of 2-iminothiolane (Traut's reagent) and MTS1 [1,1-methanediyl bis(methanethiosulfonate)]. Site-directed mutagenesis combined with chemical cross-linking revealed that residue 238 of DrABD is located within 5.4 Å from C374 of actin protomer 1 and that native cysteine 308 of drebrin is near C374 of actin protomer 2. Mass spectrometry analysis revealed that a zero-length cross-linker, 1-ethyl-3-(3-dimethylaminopropyl) carbodiimide, can link the N-terminal G–S extension of the recombinant DrABD to E99 and/or E100 on actin. Efficient cross-linking of drebrin residues 238, 248, 252, 270, and 271 to actin residue 51 was achieved with reagents of different lengths (5.4–19 Å). These results suggest that the "core" DrABD is centered on actin subdomain 2 and may adopt a folded conformation upon binding to F-actin. The results of electron microscopic reconstruction, which are in a good agreement with the cross-linking data, revealed polymorphism in DrABD binding to F-actin and suggested the existence of two binding sites. These results provide new structural insight into the previously observed competition between drebrin and several other F-actin-binding proteins.

Keywords: actin; drebrin; electron microscopy; mass spectrometry; cross-linking

*Corresponding author. E-mail address: reisler@mbi.ucla.edu.

† V.E.G., A.O., and A.J.Y. contributed equally to this work.

Current address: A. J. Ytterberg, Department of Biochemistry and Molecular Biology, University of Southern Denmark, 5230 Odense, Denmark.

Abbreviations used: ABP, actin-binding protein; mAbp1, mammalian actin-binding protein 1; DrABD, actin-binding domain of drebrin (sequence 233–317); $DrABD_{300}$, sequence 233–300 of drebrin; drADF, ADF-homology domain of drebrin (sequence 1–134); EDC, 1-ethyl-3-(3-dimethylaminopropyl) carbodiimide; EM, electron microscopic; GST, glutathione *S*-transferase; MS, mass spectrometry; MS/MS, tandem mass spectrometry; MTS, bis(methanethiosulfonate); MTS1, 1,1-methanediyl bis(methanethiosulfonate); MTS8, 3,6-dioxaoctane-1,8-diyl bis(methanethiosulfonate); MTS17, 3,6,9,12,15-pentaoxaheptadecane-1,17-diyl bis(methanethiosulfonate); SD1–SD4, subdomains 1–4; WT, wild type.

Introduction

Dendritic spines are known to be very motile and change their shape during neuronal development and in adult brain in response to various stimuli.[1] The actin cytoskeleton is a primary modulator of spine morphology. Drebrin is a filament-binding protein that is involved in organizing the dendritic pool of actin.[1] It was shown that synaptic deterioration in the brains of Alzheimer's disease patients is accompanied by dramatically decreased levels of drebrin. Reduced drebrin levels are also observed in Down syndrome.[2] Biochemical analysis of various tissues revealed that depending on specific growth state and cell density, drebrin can form higher-order oligomers named "drebrosomes," which consist of drebrin and actin alone.[3,4] It was hypothesized that such complexes allow for high local concentrations of drebrin and may play a role in the local regulation of actin assembly, as was previously shown for some tropomyosins.[5]

Drebrin binds to F-actin with a stoichiometry of one to five protomers (K_d of ~0.12 μM) and shows no actin severing, nucleating, or bundling activity *in vitro*.[6] It was previously reported that drebrins compete with F-actin-binding proteins, such as α-actinin, tropomyosin, and fascin.[6–8] Drebrin inhibits the actin-activated ATPase activity of myosin, but its effect on actomyosin sliding velocity remains unclear. A 3-fold decrease in actin sliding velocity was previously reported, but it was not confirmed in recent studies.[9,10] According to *in vitro* studies, drebrin can be displaced from actin filaments by cofilin.[11] This observation is consistent with the finding that drebrin loss is accompanied by increased levels of cofilin in the brains of Alzheimer's disease patients.[2]

Drebrin shares homology with mammalian actin-binding protein 1 (mAbp1) through an N-terminal ADF-homology domain and helical/charged motif (HCm), which is specific only to these two proteins.[12,13] However, the helical/charged motif is more extended in drebrins than in mAbp1 and contains a unique sequence (residues 233–300/317) that was identified in previous *in vivo* studies as the actin-binding domain of drebrin (DrABD) (Scheme 1).[14,15] Interestingly, this 85-amino-acid DrABD causes the same rearrangements in the actin cytoskeleton as the full-length drebrin and is highly conserved among mammals.[8,14] Both drebrin and the homologous mAbp1 are present in neuronal cells and contain an ABD within their helical/charged motif.[1,16] Nevertheless, overexpression of DrABD and the helical/charged domain of mAbp1 has different effects on the morphology and density of dendritic spines. Similar to full-length drebrin, overexpression of DrABD in rat hippocampal neurons transforms mature dendritic spine into immature dendritic filopodia (without changing the overall density of the spines) and causes the loss of synaptic contacts. This destabilizing effect of drebrin on spine morphology appears to be mediated entirely through its ABD.[8] Thus, DrABD structurally and functionally represents a unique motif among the known actin-binding modules.

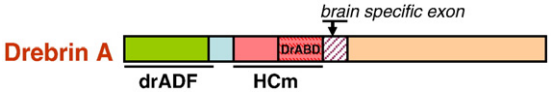

Scheme 1. Domain organization of drebrin A.

The important role of drebrin in actin regulation calls for structural understanding of the actin–drebrin complex. To date, no structural information on drebrin–actin interaction has been reported. In this study, we probed the binding interface of DrABD on actin filaments using site-directed mutagenesis, electron microscopic (EM) reconstruction, and chemical cross-linking combined with mass spectrometry (MS) analysis. Our results revealed that DrABD makes extensive contacts with subdomain 1 (SD1) and SD2 on actin and shows polymorphism in F-actin binding. Our data provide structural insight into the previously observed competition between drebrin and some of the actin side-binding proteins, such as α-actinin, cofilin, and tropomyosin.

Results

Characterization of the drebrin constructs

It was previously documented that only the N-terminal part of the drebrin molecule and DrABD in particular show actin binding and remodeling activity *in vivo*. We compared the actin binding properties of the isolated drebrin ADF-homology domain (drADF; residues 1–134), DrABD, and drebrin construct 1–300 containing both ADF and DrABD domains. Since it was previously shown that overexpression of both the 233–317 drebrin fragment (DrABD) and the 233–300 drebrin fragment ($DrABD_{300}$) causes *in vivo* effects similar to those of the full-length drebrin,[14,15] the actin binding properties of these constructs were tested under identical experimental conditions and compared with each other.

Drebrin 1–300 binds to F-actin with high affinity, K_d of ~0.2 μM (similar to that of full-sized drebrin),[6] and a binding stoichiometry of ~1:3 (Fig. 1a). Under the conditions of our experiments, the isolated drADF did not show any binding to F-actin (Fig. 1c and d).

Pelleting experiments have shown that N-GST (glutathione *S*-transferase)-fused DrABD binds to F-actin with relatively low affinity compared with the construct 1–300 (K_d = 6.6 ± 0.4 μM) (Fig. 1b). The C-terminal truncation of DrABD, to produce $DrABD_{300}$, does not affect its binding to F-actin significantly (K_d = 7.6 ± 0.6 μM). For both constructs, the DrABD/F-actin binding stoichiometry was close to 1:2 DrABD/actin protomers; the actual mole ratio (1:1.6) may reflect DrABD oligomerization, partial

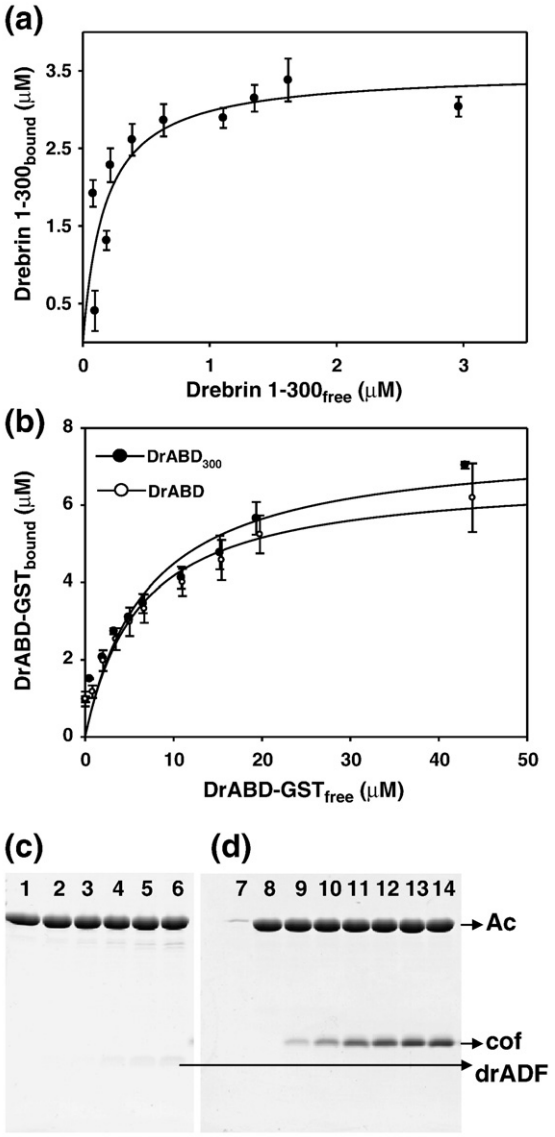

Fig. 1. Binding of the drebrin constructs to actin filaments. Binding affinity of drebrin constructs for F-actin was estimated by pelleting assays (see Materials and Methods). (a) Binding of the 1–300 drebrin construct to actin filaments (10 μM). The continuous line corresponds to the best data fit. A K_d of the 1–300 drebrin construct for F-actin (0.17±0.005 μM) was calculated based on two independent experiments. (b) Binding affinities of N-GST-fused DrABD constructs for F-actin (10 μM). Continuous lines correspond to the best data fit with K_d values of 6.6±0.4 and 7.6±0.6 μM for DrABD and $DrABD_{300}$, respectively. K_d is an average value obtained in two independent experiments, as described in Materials and Methods. (c) Co-sedimentation of drADF with F-actin (*Ac*) (10 μM). (d) Control co-sedimentation of yeast cofilin (*cof*) with F-actin (10 μM) under the same conditions as in (c). Buffer composition: 5 mM Mops, pH 7.2, 0.2 mM $CaCl_2$, 0.4 mM ethylene glycol bis(β-aminoethyl ether)*N*,*N*′-tetraacetic acid, 0.2 mM ATP, 1 mM DTT, 50 mM KCl, and 2 mM $MgCl_2$. Lanes 1–6, 10 μM F-actin co-sedimented with 1.25, 2.5, 5, 10, 15, and 25 μM concentrations of drADF; lanes 9–14, 10 μM F-actin co-sedimented with 1.25, 2.5, 5, 10, 15, and 25 μM concentrations of yeast cofilin; lanes 7 and 8, F-actin, supernatant and pellet, respectively.

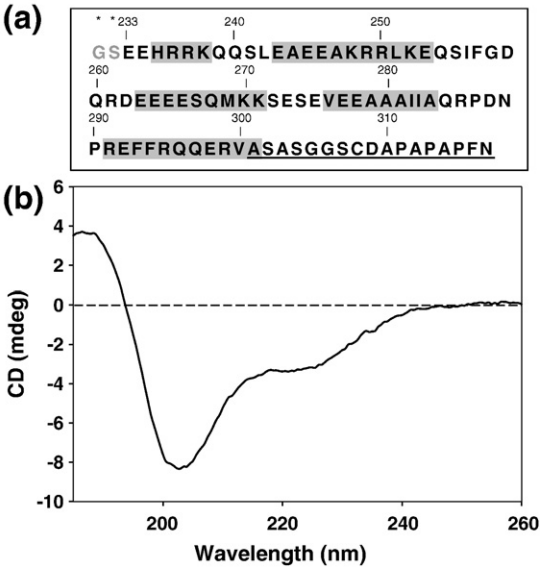

Fig. 2. Structure of DrABD. (a) Sequence of DrABD. Residues predicted to form helical structures are shown in gray (Jpred 3). The C-terminal extension that is truncated in $DrABD_{300}$ construct is underlined. Two extra amino acids at the N-terminus of the recombinant DrABD constructs are marked with asterisks. (b) CD spectrum (average of eight runs) of DrABD. Based on the results of two independent experiments, the secondary structure composition of DrABD is estimated to contain 28% helix, 15% β-sheets, and 57% turns and random coil.

occupancy of actin filament by DrABD, or its multiple binding modes (see Discussion).

DrABD has no homology among known proteins, and its sequence is abundant in glutamic acid (~19%) and arginine (~11%) (Fig. 2a). The secondary structure of this actin-binding module, as revealed by circular dichroism (CD) spectroscopy, contains 28% helix, 15% β-sheet, 21% turns, and 36% random coil (a total of 57% unstructured) (Fig. 2b). The secondary structure of DrABD is invariable over the pH range 5.0–8.6 (data not shown).

EM reconstruction of F-actin decorated with the drebrin constructs

EM images of F-actin alone and actin decorated with DrABD and 1–300 constructs are shown in Fig. 3a, b, and b*, respectively. Despite affinity differences, the same modes of F-actin binding and binding polymorphism were documented for both DrABD (Fig. 3d–h) and drebrin 1–300 constructs (Fig. 3d*–h*).

Extensive decoration of actin filaments was observed in the presence of DrABD (Fig. 3b), as well as with the shorter construct $DrABD_{300}$ and N-GST-fused DrABD (data not shown). We collected 9749 segments from images of actin filaments decorated with the drebrin fragment. During the first step of sorting, segments were separated by the occupancy (see Materials and Methods and Appendix A) and

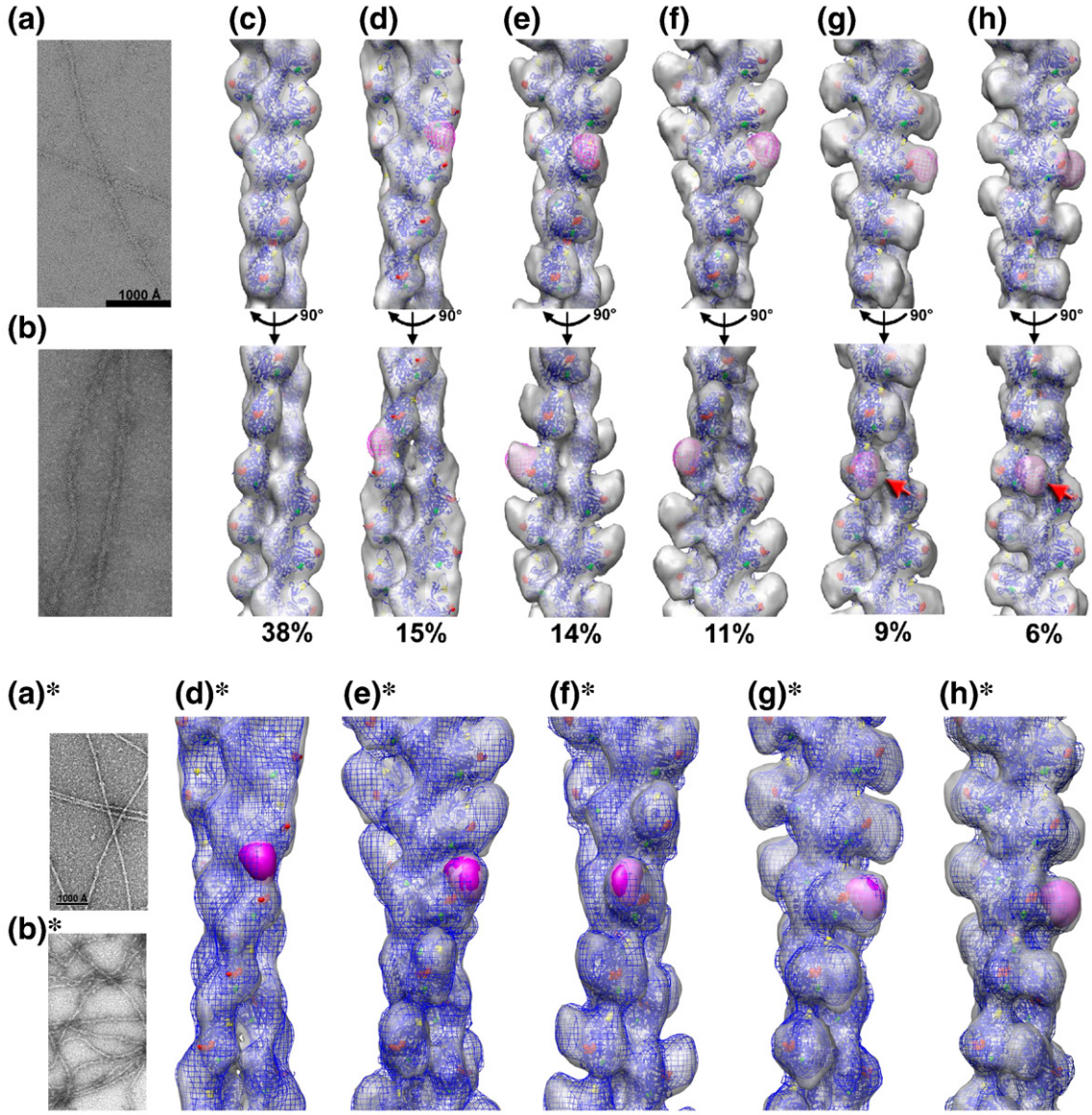

Fig. 3. EM and three-dimensional reconstruction of the drebrin–F-actin complex. (a, a*, b, b*) Electron micrographs of F-actin alone (a and a*), filaments decorated with the DrABD construct (b), and those decorated with the drebrin 1–300 construct (b*). (c–h) Three-dimensional reconstructions of pure F-actin (c) and five modes of binding of drebrin to F-actin (d–h). Atomic model of actin filament docked into each map is shown as blue ribbons (c–h). F-actin residues 99 and 100 (red), 51 (yellow), and 374 (green) are shown as spheres (c–h). (d–h) An electron density envelope that corresponds to a globular protein containing 84 amino acid residues is shown as magenta meshwork. (d*–h*) Comparison of the binding modes of DrABD and drebrin 1–300 construct to F-actin. Reconstructions of F-actin decorated with DrABD are shown as transparent surfaces, while volumes that resulted from filaments complexed with the 1–300 construct containing both DrABD and AFD-homology domain are shown as blue meshwork. Atomic model of actin filament docked into each map is shown as blue ribbons (d*–h*). F-actin residues 99 and 100 (red), 51 (yellow), and 374 (green) are shown as spheres (a–e). An electron density envelope that corresponds to a globular protein composed of 84 amino acid residues is shown as magenta solid surface. The modes of binding obtained for drebrin 1–300 construct are similar to the ones observed for isolated DrABD.

"naked" F-actin segments were reconstructed separately from occupied ones. Reconstruction of the naked F-actin (Fig. 3c) was similar to the reconstruction of pure F-actin from our previous studies.[17] Five modes of DrABD binding to actin filaments are shown in Fig. 3d–h. To estimate whether the observed additional mass in the reconstructions was consistent with the molecular weight of the drebrin construct, we used a portion of the globular CH domain of α-actinin (Protein Data Bank ID 1wku) that consists of 84 residues (~9 kDa). This model protein fragment was filtered to ~24-Å resolution, and its expected molecular volume was docked into the drebrin density in each map (Fig. 3d–h, magenta mesh). In the first mode (Fig. 3d), drebrin bridges to two adjacent actin

protomers and makes an extensive contact with SD1 and SD2. In the mode shown in Fig. 3e, drebrin is located in front of actin SD1. We also observed drebrin in a mode similar to the one shown in Fig. 3d, but in this mode, DrABD interacts with one protomer at a time (Fig. 3f). We suggest that all three modes shown in Fig. 3d, e, and f are variations of a major DrABD binding site (~40% of segments), which involves SD1 and SD2 of actin.

We found that ~15% of the segments decorated with DrABD reflect a different type of attachment (Fig. 3g and h). In the binding mode shown in Fig. 3g, DrABD is attached to the sides of SD1 and SD2. In this case, the observed mass was larger than the mass corresponding to a globular protein fragment of 84 amino acids, which suggests that, in this mode, DrABD binds to filaments as an oligomer. Interestingly, in this mode, DrABD makes contact with SD4 of an actin protomer on the opposite strand (Fig. 3g, red arrow). This contact is more prominent in the mode shown in Fig. 3h.

The same modes of binding as documented for DrABD were also observed for the 1–300 construct, despite its much higher affinity for F-actin (~0.2 μM) (Figs. 1a and 3d*–h*). It should be noted that the 1–300 construct may contain weak actin-interacting sites other than DrABD, which would explain its higher affinity for the actin filaments. However, the results of EM reconstruction suggest that DrABD contains the strongest binding site within the 1–300 drebrin fragment and probably competes with weaker bound structural elements for interaction with actin when the 1–300 fragment is added in excess. Based on our EM results and previous *in vivo* studies, the DrABD construct was chosen for mapping the drebrin binding site on F-actin.

DrABD bridges two actin protomers

To probe the DrABD/F-actin binding interface via cross-linking reactions, we employed the modification of DrABD with 2-iminothiolane (Traut's reagent). This reagent was used to introduce sulfhydryl (-SH) groups on the surface of the fragment. Potentially, all five lysines (K238, K248, K252, K270, and K271) and the N-terminal amino group can be modified with 2-iminothiolane. Additionally, DrABD contains native cysteine 308 within its C-terminal unstructured extension (residues 301–317). Considering the relatively low affinity of DrABD to actin, we attached first the cross-linking reagents to F-actin, as was done earlier for the mapping of the actin–thymosin β4 complex.[18] Cross-linking experiments revealed that DrABD modified with Traut's reagent can be covalently attached to MTS1 [1,1-methanediyl bis (methanethiosulfonate)]-pre-modified F-actin, yielding two protein populations: actin–DrABD heterodimer and species that, according to their molecular weight, correspond to a complex of two actin protomers and one DrABD molecule (Fig. 4a). A control experiment was carried out using MTS1-pre-modified F-actin and intact DrABD construct with no modifications. A significant amount of actin–DrABD heterodimer was detected by SDS-PAGE under nonreducing conditions, indicating that native C308 on DrABD is involved in the cross-linking (Fig. 4b).

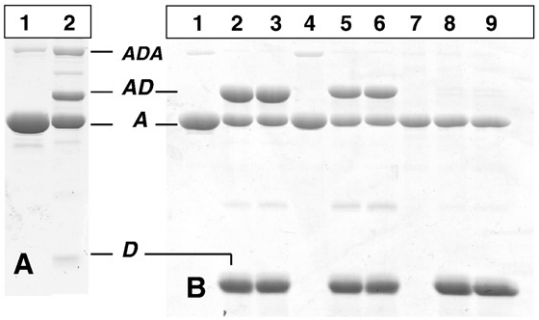

Fig. 4. DrABD is near the C-terminal regions of two adjacent actin protomers. (a) DrABD treated with 2-iminothiolane (Traut's reagent) can be covalently attached to MTS1-pre-modified skeletal F-actin: lane 1, MTS1-modified F-actin (10 μM) (*A*); lane 2, 2-iminothiolane-treated DrABD (20 μM) incubated for 5 min with MTS1-modified actin. Two main cross-linking products were detected: actin–DrABD heterodimer (*AD*) and the species that, according to molecular weight and MS analysis, corresponds to two actin protomers and one DrABD (*ADA*). (b) Native C308 of DrABD is within 5.4 Å from C374 on actin: lanes 1–3, skeletal F-actin; lanes 4–6, WT yeast actin; lanes 7–9, yeast actin mutant C374A. Lanes 1, 4, 7, MTS1-modified actins; lanes 2, 5, and 8, MTS1-modified actins in the presence of DrABD (5-min reaction time); lanes 3, 6, and 9, same as lanes 2, 5, and 8 but with 17-min reaction time. The final concentrations of actin and DrABD were 9.5 and 28.5 μM, respectively.

C-terminal region of DrABD (residues 301–317) cross-links to C374 on actin

Our experiments revealed that DrABD can be efficiently cross-linked to both skeletal muscle (α-) and yeast wild-type (WT) (cytoplasmic) F-actin pre-modified with MTS1. The similar cross-linking yield (~60%) obtained for both actins may indicate that the DrABD–actin interaction is not isoform specific. C-terminal cysteine 374 is the most reactive cysteine on actin and is expected to be efficiently modified with MTS1 reagents.[19] However, to confirm that the cross-linking on actin indeed involves C374, we used a yeast actin mutant with this residue substituted to alanine (C374A). No cross-linking was detected in the case of C374A actin mutant, which indicates that native C308 of drebrin locates within 5.4 Å from C-terminal cysteine 374 on actin (Fig. 4b).

MS analysis of the purified complex of 2-iminothiolane-modified DrABD attached simultaneously to two actin protomers revealed that disulfide (MTS1) cross-linking between native C308 on DrABD and C10 on actin may also occur (Appendix B). However, the fact that unmodified DrABD can be efficiently cross-linked to WT yeast actin, which lacks C10, suggests that this type of attachment reflects a minor mode of DrABD–actin binding.

The N-terminal part (233–271) of DrABD can be cross-linked to SD1 and SD2 of two adjacent actin protomers

Site-directed mutagenesis was employed to locate the N-terminal part of DrABD (sequence 233–271) on actin filaments. Based on the results obtained with 2-iminothiolane-modified DrABD (Fig. 5a), all five lysines (K238, K248, K252, K270, and K271) and the N-terminal glycine were potential candidates for cross-linking to the second actin protomer. To identify the residues on DrABD that are in close proximity actin, we created five mutants with single lysine-to-cysteine replacements in the construct $DrABD_{300}$. These mutants did not impair the complex formation of $DrABD_{300}$ with F-actin (see Materials and Methods). The fact that DrABD bridges two actin protomers, making contacts with their C-terminal segments, called for probing the DrABD interaction with actin SD2. Actin mutants D51C/C374S and S60C/C374A were employed for such mapping. Mutant A144C/C374A was chosen to test for the binding of DrABD to the hydrophobic cleft between SD1 and SD3 of actin, which is known to interact with several actin-binding proteins (ABPs). All yeast actin mutants employed in this study show normal polymerization properties.[20,21]

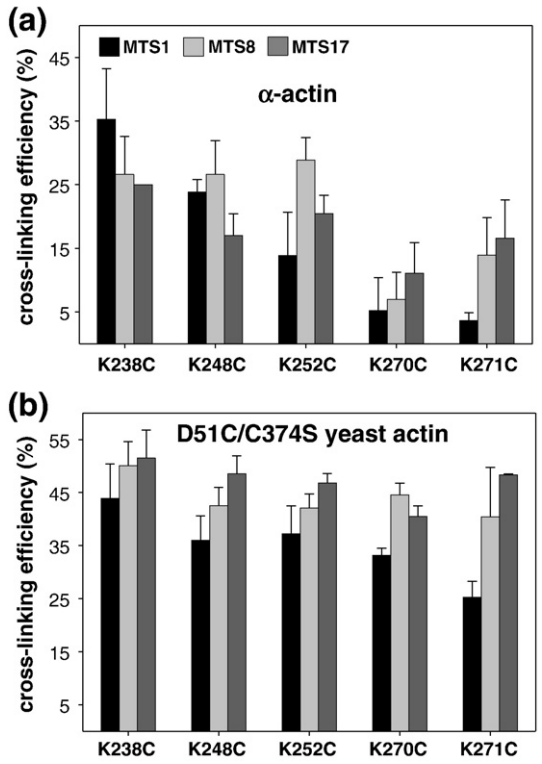

Fig. 5. Mapping DrABD binding interface on F-actin. (a and b) Thiol-specific cross-linking of five DrABD mutants to skeletal F-actin (a) or to yeast actin mutant D51C/C374S (b) modified with MTS reagents of different lengths. Residue 238 of drebrin is within 5.4 Å from the Cys374 of actin (C-terminus). Residues 238, 248, 252, 270, and 271 of drebrin are within ~12.1 Å from residue 51 on actin (D-loop, SD2). F-actin was pre-modified with MTS immediately prior to the cross-linking. The final concentrations of actin and DrABD were 10 and 30 μM, respectively. The reactions were stopped with *N*-ethyl maleimide after 5 min, and the resulting mixtures were analyzed by SDS-PAGE. Relative intensities of protein bands were determined by densitometric analysis. Cross-linking efficiencies were estimated as follows: [Actin Total (Before the Reaction) − Uncross-Linked Actin Monomer Left After 5 Min]/Total Actin, (%). Black, MTS1 (5.4 Å); light gray, MTS8 (12.1 Å); dark gray, MTS17 (19 Å).

We used a series of bis(methanethiosulfonate) (MTS) reagents as molecular rulers to estimate the distances between single reactive cysteines on actin and on DrABD mutants.[21] Experiments with skeletal F-actin pre-modified with MTS1 (5.4 Å) revealed that K238C is the one cross-linked most efficiently to C374 on actin among the five $DrABD_{300}$ mutants (Fig. 5a). The cross-linking yields for three DrABD mutants, K238C, K248C, and K252C, and the MTS8 [3,6-dioxaoctane-1,8-diyl bis(methanethiosulfonate)]-pre-modified F-actin were very similar (27%–29%). These results suggest that lysines 238, 248, and 252 are in close enough proximity to C374 of actin (~12 Å) to be involved in the formation of a trimer consisting of 2-iminothiolane-modified DrABD attached simultaneously to two actin protomers (Fig. 4a). The low cross-linking efficiency documented for mutants K270C and K271C and actin pre-modified with the MTS reagents of different lengths precludes their proximity to C374 on actin (Fig. 5a).

The experiments with MTS-modified yeast actin D51C/C374S revealed that all five $DrABD_{300}$ mutants could be linked very efficiently to actin with reagents of length ranging from ~12.1 Å (MTS8) to 19 Å [MTS17; 3,6,9,12,15-pentaoxaheptadecane-1,17-diyl bis(methanethiosulfonate)] (Fig. 5b). These data indicate that the N-terminal part of DrABD is centered on SD2 of actin. However, in the case of MTS1-modified D51C/C374S actin, the cross-linking efficiency of the introduced cysteine residues decreases with increasing distance from the N-terminus of the DrABD construct (Fig. 5b). The fact that all five $DrABD_{300}$ mutants can be cross-linked efficiently to residue 51 on actin may indicate that the construct can adopt a folded conformation upon binding to F-actin.

No cross-linking was detected with all five $DrABD_{300}$ mutants and yeast actin S60C/C374S, with the reactive cysteine in SD2 facing the nucleotide binding cleft, and yeast actin A144C/C374A, containing a reactive cysteine in the hydrophobic cleft (SD3) of actin (data not shown).

Zero-length cross-linking of DrABD to SD1 of actin

Our experiments showed that DrABD can be efficiently cross-linked to F-actin using the zero-length cross-linker 1-ethyl-3-(3-dimethylaminopropyl) carbodiimide (EDC) (Fig. 6a; Appendix C). Bands corresponding to actin, DrABD, and actin–DrABD heterodimer were excised from the SDS-PAGE gel and subjected to in-gel trypsin digest to

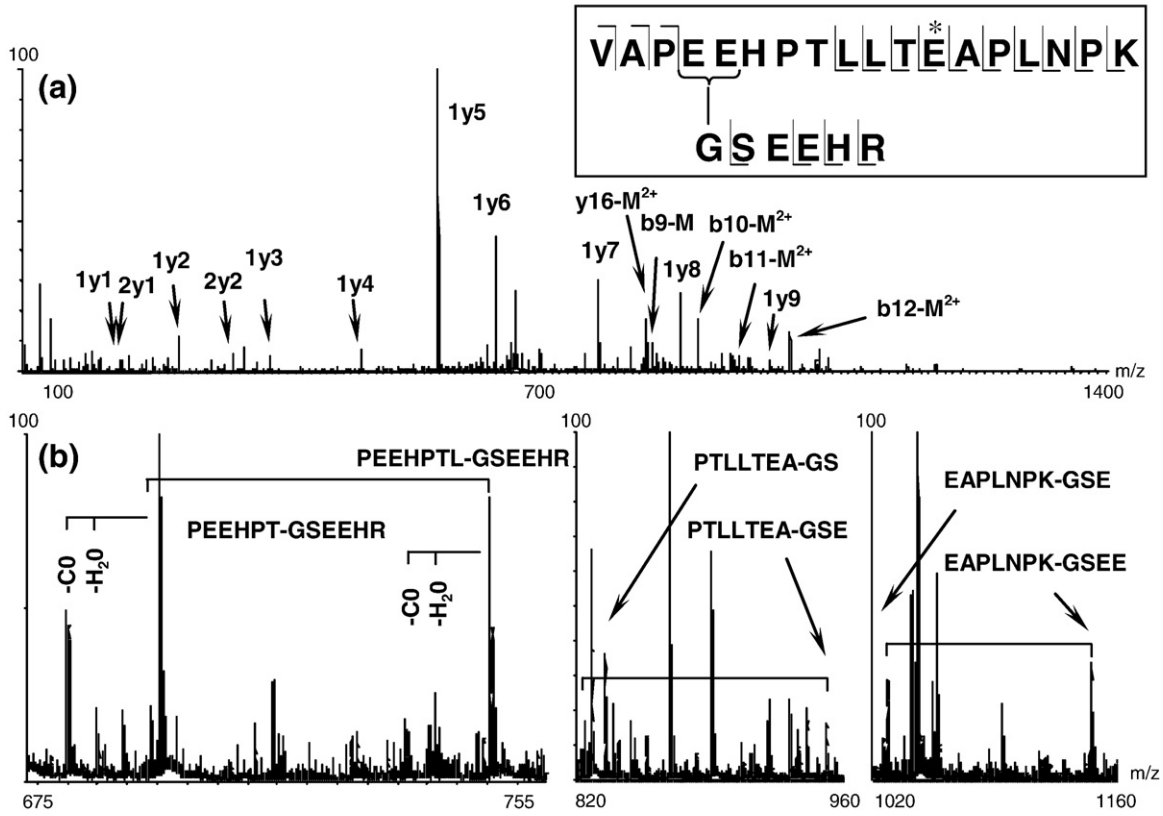

Fig. 6. N-terminus of DrABD constructs can be attached to SD1 of actin with the zero-length cross-linking reagent EDC. (a) Tryptic peptides of DrABD–actin heterodimer were analyzed by MS/MS. The 663.61 $(M+4H)^{4+}$ peak in MS spectra, corresponding to cross-linked peptides, was fragmented using electrospray ionization MS/MS (Waters Synapt QTOF mass spectrometer). Some of the identified fragments are indicated in the figure. The first digit indicates the peptide from which the fragment originates (1 = actin, 2 = drebrin), the letter refers to the ion series, and the last digit represents the ion number. Hyphenated labels indicate cross-linked fragments, with the left fragment originating from actin and the right one from drebrin. "M" represents intact drebrin peptide. The inset shows a schematic representation of the cross-linked peptides. In the scheme, the cross-linked residues are connected with a continuous line (major site); a minor cross-linking site on actin peptide is marked by the asterisk. (b) Internal ions of the cross-linked peptides support the attachment of N-terminal Gly of DrABD to E99/E100 (major population) and E107 (minor cross-link) on actin.

map the cross-linked sites. Cleavage products were analyzed by electrospray ionization tandem MS (MS/MS). A peptide ion ($[M+4H]^{4+} = m/z$ 663.61) unique to the cross-linked heterodimer was fragmented by MS/MS and matched to the two cross-linked peptides: actin 96–113 and drebrin 233–236, containing extra G–S extension at the N-terminus. The fragments were deconvoluted to a zero-charge spectrum and matched with theoretical masses predicted for the three cross-linking sites on the actin peptide (E99, E100, and E107) and the single cross-linking site on drebrin (the N-terminus) to fully assign the spectrum. The data were first filtered using a maximum error of ±100 ppm to ensure high quality of the matches. In a second filtering step, the average and standard deviation of the errors were calculated and one standard deviation from the average (27±37 ppm) was used as a filter. The identified fragments were then matched with the raw spectrum to increase the confidence by using the multiple charge states of each fragment. Fifty-seven fragments were found with unique interpretations (24 had two or more charge states), 11 fragments matched to sequences occurring more than once in the peptide sequence, and 16 ions could be matched to more than one fragment (within experimental error). To assign the latter to single fragments, we evaluated the number of fragmentations necessary to form the fragment and the presence of supporting ions from related fragments. The mass-to-charge ratio (m/z) and the charge of each fragment were manually verified from the raw spectrum. The interpretation of the data fits with a cleavage of 24 bonds, out of 26. Twenty-one fragments support a cross-link at E99 or E100 located in SD1 (major population) of actin, while 6 fragments (i.e., a minor population) support a cross-link at E107 (Fig. 6b; Appendix C).

Discussion

In order to identify contact sites between actin and drebrin, we employed site-directed mutagenesis, EM reconstruction, chemical cross-linking, and MS analysis. Using a set of thiol-specific reagents of different lengths as molecular rulers, we were able to assign the distances between selected residues on

actin and DrABD in the range of 0 to ~19 Å. The results of EM reconstruction revealed polymorphism in DrABD binding to actin filaments and suggested the existence of at least two binding sites for DrABD.

The contents of helical and β-structures estimated for DrABD using CD spectroscopy were 28% and 15%, respectively. However, secondary structure prediction algorithms did not predict any β-structures in DrABD (Fig. 2). Our current crystallization attempts, if successful, would resolve this contradiction. The level of random coil and turns estimated by CD (57%) was in good agreement with the predictions made by Jpred 3 (~50%), which suggests proper folding.[22] The affinity of DrABD for F-actin determined by pelleting experiments (K_d of ~6.6–7.6 μM) was relatively low compared with the affinity reported for the full-length drebrin (0.12 μM).[6] Our observation that drebrin construct 1–300 has a significantly higher affinity for F-actin compared with DrABD (~0.2 μM; Fig. 1) raises the possibility that regions other than DrABD may also contribute to the actin binding. We hypothesize that either the ADF-homology domain or the linker region (residues 143–232) contributes to the stronger binding of drebrin 1–300 to F-actin than that of DrABD. Our EM reconstruction results (see below) suggest that DrABD is the strongest actin binding region within the 1–300 drebrin fragment, and identification of weaker binding sites is a subject for a separate study.

The fact that the shorter construct of $DrABD_{300}$ (with deletion of 17 C-terminal amino acids) has approximately the same affinity to F-actin as the longer construct (sequence 233–317) indicates that the unstructured region 301–317 does not contribute significantly to the DrABD/F-actin interaction (Fig. 1b).

Chemical cross-linking for mapping the protein binding interface

Several DrABD and actin mutants containing single reactive cysteines were reacted with a series of thiol-specific bifunctional MTS reagents to probe the actin–DrABD binding interface. In general, the cross-linking efficiency depends on the reactivity and accessibility of the targeted residues, stability of the cross-linking reagents in solution, and experimental conditions (pH, temperature, reaction time).

The results of our cross-linking and pelleting experiments suggest that DrABD bridges two adjacent actin protomers. However, these data are insufficient to determine the orientation of DrABD on actin filaments. Based on our results summarized in Fig. 7, we discuss the interaction of DrABD with protomers 1 and 2 in the actin filament.[23]

Cross-linking of DrABD to actin SD1 (protomer 1)

After thrombin cleavage, the recombinant DrABD constructs contain a G–S N-terminal extension. MS analysis identified the N-terminal glycine on DrABD as a residue cross-linked to F-actin with a zero-length cross-linking reagent (EDC) (Appendix C). On actin, three residues in SD1 were shown to be involved in EDC cross-linking with DrABD: E99 and/or E100 (major population) and E107 (minor population) (Fig. 6). Although a distinction between cross-linking to E99 and E100 is not possible from the fragmentation pattern of the cross-linked peptides, we conclude based on the abundance of the internal fragments of the cross-linked peptides that DrABD cross-linking to E107 of actin represents a minor population. The analysis performed using GETAREA 1.0 software showed a significant decrease in solvent accessibility for actin residue E107 compared with E99 and 100. Based on that, we cannot rule out the possibility that the N-terminus of DrABD is flexible and locates in close proximity to all three residues (E100, E99, and E107) but its coupling to E107 is restricted by the accessibility of that residue. It is also conceivable that minor cross-linking to E107 of actin may reflect an alternative mode of DrABD binding or result from local damage to actin over the course of the reaction. Despite the high level of flexibility of DrABD in solution (our unpublished NMR data) and the predicted disordered state of its N-terminal region, only one cross-linked peptide was identified in the sample containing the DrABD–actin

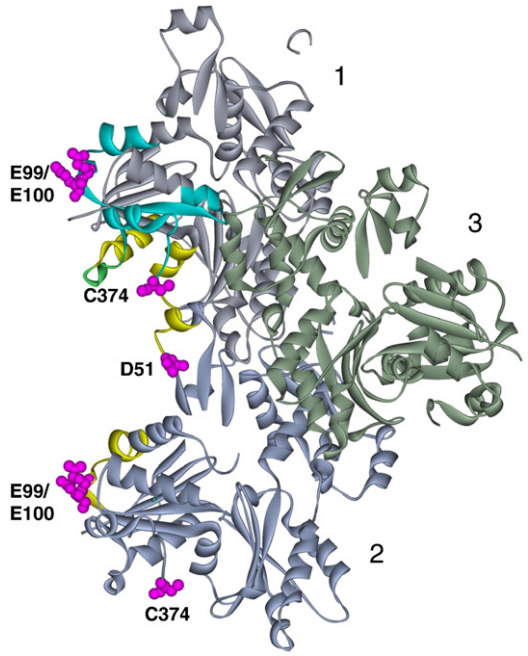

Fig. 7. Summary of the cross-linking results. Holmes model of actin filament structure.[23] Actin protomers are marked as 1, 2, and 3. Actin residues involved in cross-linking with DrABD are shown in magenta. Actin peptides involved in interactions with cofilin[17] and α-actinin[24] are shown in yellow and blue (protomer 1), respectively. The overlap between cofilin and α-actinin binding sites is shown in green (protomer 1).

heterodimer, which indicates a specific DrABD interaction with the 99–107 actin region.

Cross-linking experiments employing skeletal α-actin pre-modified with MTS reagents and DrABD mutants containing single cysteine substitutions revealed that the N-terminal part of DrABD makes contact with the C-terminus of actin. Based on the highest cross-linking efficiency of the K238C mutant to MTS1-modified actin, we conclude that residue 238 of DrABD locates within ~5.4 Å from C374 of actin (Fig. 5a). The fact that longer-spanning reagents [MTS8 (12.1 Å) and MTS17 (19 Å)] cross-link the same K238C mutant to actin at lower efficiency may indicate that, in the extended conformation, these reagents do not fit well into the space between the two cysteine residues in the DrABD–actin complex, while the "*gauche*" conformations of the reagents may not have the appropriate geometry for bridging residues 374 and 238. Similar amounts of actin–DrABD heterodimer were obtained in the presence of mutants K238C, K248C, and K252C with MTS8, which indicates that these three residues are within ~12 Å from the C-terminus of actin. Low cross-linking efficiency between C374 of actin and DrABD mutants C270 and C271 observed with the MTS reagents of different lengths indicates that those residues are distant from the C-terminus of actin (Fig. 5a).

Cross-linking of DrABD to actin SD1 and SD2 (protomer 2)

Experiments with yeast actin mutant D51C/C374S containing a single reactive cysteine in SD2 revealed that DrABD is close to this actin region. Residues 238, 248, 252, 270, and 271 on DrABD can all be efficiently attached to residue 51 on actin with MTS reagents of various lengths (5.4–19 Å) (Fig. 5b). The efficiency of these reactions with MTS1 and MTS8 is slightly higher (by ~8%) for the DrABD mutant K238C (Fig. 5b). According to secondary structure predictions, lysines 248 and 252 of DrABD are located on a helix, and lower cross-linking efficiency for these mutants, compared with K238C, may indicate decreased solvent accessibility of these two residues. Our results indicate that all five lysines on DrABD are located within ~12 Å or even closer (5.4 Å in the case of K238) residue 51 on actin.

Our cross-linking experiments also revealed that the C-terminal region of DrABD interacts with actin SD1 and that native cysteine 308 of drebrin locates within 5.4 Å from C374 on actin (Fig. 4b). Minor cross-linking between C10 on actin and C308 on DrABD may reflect the flexibility of the C-terminal region of the DrABD construct, but it could also indicate an alternative binding mode (Appendix B).

EM reconstruction of F-actin decorated with DrABD is consistent with cross-linking results

We used a single-particle approach for the EM reconstruction of F-actin decorated with DrABD.[25] This method allows for sorting relatively short filament segments (~400 Å long) by occupancy and the mode of drebrin binding to F-actin.

In four modes of binding (Fig. 3d–f and h), the mass attributed to DrABD is consistent with a globular protein of ~9 kDa attached to F-actin. The results of EM reconstruction together with the mapped location of residues 238, 248, 252, 270, and 271 on DrABD within ~12 Å from residue 51 on actin lead to the conclusion that DrABD may adopt a globular conformation upon binding to actin. Our data suggest that in the modes presented in Fig. 3d–f and h, DrABD binds to F-actin predominantly as a monomer. However, we cannot exclude the possibility that in these four modes actin filaments are decorated by drebrin dimers/oligomers, which are not observed due to low occupancy or disorder.

According to the EM reconstruction and in good agreement with our cross-linking results, DrABD makes extensive contacts with SD1 and SD2 of actin (Fig. 3). In the modes presented in Fig. 3d and f, DrABD interacts with SD1 and SD2 that involves residues 51 and 99–100. In the mode shown in Fig. 3e, DrABD is located in front of SD1 of actin and the interface involves residues 99 and 100. In the minor binding mode presented in Fig. 3g, residues 51, 99, 100, and 374 are in proximity to DrABD density. Also, in the mode presented in Fig. 3h, residues 51 and 374 are likely to be involved in the interaction with drebrin. Taken together, the EM data support the existence of two binding sites for DrABD on actin: a major site (modes shown in Fig. 3d–f, ~40% segments) and a minor site (modes shown in Fig. 3g and h, ~15% segments) where DrABD is shifted to the sides of SD1 and SD2 of actin and makes cross-strand contact with another actin protomer.

Our cross-linking experiments revealed that DrABD can be simultaneously attached to two adjacent actin protomers within one helical strand. According to our mapping, C374 residues on two adjacent protomers are involved in such double cross-linking, which appears to be inconsistent with the results of EM reconstruction (Figs. 4 and 5a). However, it should be noted that the C-terminal extension of DrABD that cross-links to C374 of actin with MTS1 (Fig. 4b) is predicted to be unstructured. Computational analysis performed using Insight II software revealed that the length of this C-terminal extension (amino acids 301–317, C^{α} to C^{α}) spans between 4.7 and 26.7 Å. If this region is disordered, it would not be observed in the EM reconstructions. According to our MS analysis, a short N-terminal extension of DrABD makes contact with actin residues 99–100. We may speculate that DrABD consists of a helical core with the unstructured extensions docked to the SD1 regions of two adjacent actin protomers. An atomic-resolution structure of the DrABD–actin complex will be required to confirm this hypothesis.

Polymorphism of DrABD binding to actin: implications for competition with other ABPs

Along with drebrins, many other ABPs are involved in the regulation of the actin cytoskeleton in neuronal cells. At the molecular level, the interplay between ABPs in this system is poorly understood. Our results provide new structural insight into the reciprocal relationship between drebrin and other ABPs in the cell. Multiple binding modes to F-actin documented here for DrABD were reported earlier for other proteins, such as cofilin,[17] utrophin,[26] and tropomyosin.[27–30] Thus, binding polymorphism is not an exception among actin-interacting proteins and may play an important role in actin cytoskeletal regulation. Because construct 1–300 of drebrin binds to F-actin significantly tighter than DrABD yet shows the same modes of attachment to actin filaments (Figs. 1a and 3d*–h*), the *in vivo* competition of DrABD with other ABPs would be functionally important.

This study revealed that the main DrABD binding site overlaps with the cofilin binding site on actin filaments, which would explain the competition between these two proteins.[11] Cofilin interacts with two actin protomers within the same helical strand: with an upper protomer at the hydrophobic cleft between SD1 and SD3 and with a lower protomer at the interface formed by SD1 and SD2. On the lower protomer, peptides 44–50, 28–29, and 88–101 appear to be involved in cofilin binding (F-binding site).[17,31] On the upper protomer, the C-terminus of actin was shown to interact with cofilin.[21,32] Thus, our mapping of DrABD sites on actin to regions proximal to residues D51, E99, E100 and the C-terminus indicates their overlap with the cofilin binding site.

It has been shown that drebrin overexpression causes displacement of α-actinin from dendritic spines, which is consistent with earlier *in vitro* observations.[8] An α-actinin was documented previously to interact with residues 86–117 and 350–375 on actin.[24] We have shown here that actin residues 99–107 and its C-terminus are near DrABD, explaining the previously observed competition between these two proteins. According to the *in vitro* studies, α-actinin can interact with both F-actin (through tandem CH domains) and NMDA receptors (through its central "rod" domain), anchoring actin filaments to the membrane.[33,34] It is likely that the competition between drebrin and α-actinin affects the anchoring of actin filaments to the membrane and leads to the formation of the long protrusions observed upon drebrin overexpression. We may hypothesize that the observed polymorphism of DrABD binding to F-actin plays a role in the competition with spectrin family proteins, such as utrophin, which have multiple actin-binding modes.[26]

Based on *in vitro* studies, it was suggested that drebrin and tropomyosin compete for the same actin binding site. In the absence of atomic-resolution structures, the detailed mechanism of such competition remains unclear. Also, we cannot exclude that observed inhibition of drebrin binding occurs due to tropomyosin-induced conformational changes in F-actin. Our data suggest that the primary binding site of drebrin (Fig. 3d–f) is inconsistent with simultaneous interaction of drebrin and myosin with F-actin because myosin binds to a similar interface on F-actin.[35] It is possible that the attachment of F-actin decorated by drebrin A to a glass surface coated with myosin-V occurs because of the shift of DrABD from its primary binding site to the minor one located on the side of the filament.[10]

Materials and Methods

Materials

MTS cross-linking reagents, MTS1, MTS8, and MTS17, were purchased from Toronto Research Chemicals (North York, Ontario, Canada). Millipore-filtered water and analytical-grade reagents were used in all experiments.

Molecular cloning and mutagenesis

Mouse (*Mus musculus*) brain RNA was purified using TRIzol reagent (Invitrogen). Reverse transcriptase-PCR was performed using SuperScript II (Invitrogen) to generate cDNA. Full-length drebrin A cDNA was cloned into pCR2.1-TOPO vector (Invitrogen) and used as a template for all drebrin constructs. DrABD was cloned into BamH1 and EcoR1 sites of pGEX-4T1 expression vector. $DrABD_{300}$ construct was created by introducing a stop codon after amino acid 300 (Val) in DrABD with a QuikChange kit (Stratagene). DrABD mutants K238C, K248C, K252C, K270C, and K271C that contain single lysine-to-cysteine replacements were created using the same kit. Drebrin construct 1–300 was obtained by introducing a stop codon after residue 300 in full-length drebrin A DNA subcloned into pGEX-4T1 expression vector. The primers for cloning and mutagenesis are given in Appendix D.

Protein expression and purification

Rabbit skeletal actin was purified from rabbit back muscle as described by Spudich and Watt.[36] Yeast actin was purified as described previously.[21] All drebrin ABD constructs were expressed in Rosetta cells. Cells were grown at 37 °C until $OD_{600} = 0.6–0.8$, following the induction with 0.2 mM IPTG and 2 h of expression. Proteins were purified on glutathione-agarose according to the manufacturer's instructions and as detailed in Appendix A. The single cysteine mutations introduced into $DrABD_{300}$ construct did not impair its complex formation with F-actin (Fig. 8). Consequently, we employed these mutants for mapping the drebrin interface on actin.

Actin polymerization and DrABD binding assays

Actin polymerization was monitored via light scattering with the PTI fluorometer set at 350 nm for the excitation and emission wavelengths. For pelleting experiments,

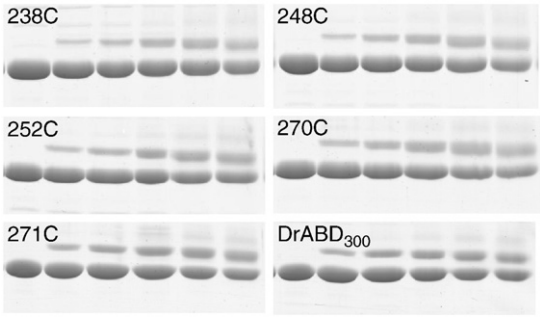

Fig. 8. Single cysteine substitutions introduced into DrABD do not impair its ability to bind F-actin. Time course of cross-linking reactions (0, 5, 10, 20, 40, and 75 min) between skeletal F-actin (10 μM) and $DrABD_{300}$ mutants (30 μM) in the presence of EDC (30 μM). The higher mobility bands correspond to actin, whereas the lower mobility bands represent the cross-linked actin–DrABD complex. Reaction conditions: 5 mM Mops, pH 7.2, 0.2 mM $CaCl_2$, 0.2 mM ATP, 0.11 mM TCEP, 100 mM KCl, and 2 mM $MgCl_2$.

polymerization of skeletal actin was induced by addition of 2.0 mM $MgCl_2$ and 100 mM KCl to the actin solution in 5 mM Tris, pH 8.0, 0.2 mM $CaCl_2$, 0.2 mM ATP, and 5 mM β-mercaptoethanol. The samples were centrifuged at 312,500*g* for 30 min, at 4 °C, in a Beckman TLA-100 rotor. Resulting pellets were solubilized in gel sample buffer and analyzed by SDS-PAGE. To quantify the amount of N-GST-fused DrABD co-sedimented with F-actin, we loaded 0.4–3.6 μg of purified constructs on each gel as the standards. Gels were stained with Coomassie Blue. The intensities of the bands were estimated using Scion Image Software. Binding parameters (K_d and B_{max}) were obtained by fitting the average data points in SigmaPlot 9.0. The resulting curves (Fig. 1) represent the best fit.

Actin modification and cross-linking

Immediately prior to the reaction, DTT was removed from G-actin samples over a Sephadex G-50 spin column equilibrated with thiol-free buffer containing 5 mM Mops, pH 7.2, 0.2 $CaCl_2$, and 0.2 mM ATP. Drebrin ABD constructs were passed through a Zeba Desalt Spin Column (Pierce) equilibrated with the same buffer. Actin was polymerized in the presence of 2.0–3.0 mM $MgCl_2$ and 100 mM KCl. The reactions of F-actin modification with MTS were carried out at room temperature (1–10 min), at molar ratios of 0.95:1 of MTS/actin. Cross-linking reaction was started by mixing DrABD constructs with MTS-pre-modified F-actin. Aliquots were withdrawn from the reaction mixtures at selected time points, and free cysteine residues were blocked with *N*-ethyl maleimide. Cross-linking progress was monitored by SDS-PAGE under nonreducing conditions.

Circular dichroism

CD spectra of DrABD (0.5 mg/ml) in 5 mM Tris, pH 7.8, at 25 °C were measured using a J-700 polarimeter (Jasco). Eight replicates of each spectrum were recorded using scanning speed of 20 nm/min, a data pitch of 0.5 nm, and a 4-s dwell time. Samples were measured in a quartz cuvette with a path length of 0.01 cm. CD spectra were deconvoluted using the Selcon3 algorithm. Secondary structure obtained from the CD spectra was compared with that calculated from the secondary structure prediction algorithm Jpred 3.

MS and data analysis

Actin, DrABD, and EDC cross-linked heterodimers were separated using PAGE. The gel bands were digested as described previously.[37] Actin, DrABD, and the trimer, consisting of 2-iminothiolane-modified DrABD attached to two adjacent protomers through MTS1, were separated using size-exclusion chromatography and digested in-solution as described earlier[38] and detailed in the Appendix A. The peptides were first analyzed by matrix-assisted laser desorption/ionization time-of-flight MS (Voyager DE-STR, Applied Biosystems, Framingham, MA), using the dried droplet method with dihydroxybenzoic acid as matrix, and then by MS/MS. The digests were desalted using microcolumns[39] packed with POROS R2 beads (Applied Biosystems) and eluted directly into glass capillaries (Proxeon Biosystems, Odense, Denmark) to be analyzed manually by MS/MS (Synapt HDMS, Manchester, UK).

Spectra for the unmodified samples were acquired first and then used as controls during the analysis of the cross-linked sample to determine unique peptide ions. In each analysis, a few relevant peptides were analyzed, each up to 25 min to ensure high spectrum quality. A small portion of the sample, cross-linked using MTS1, was incubated with 10 mM DTT for 1 h and analyzed by MS/MS to verify the disulfide nature of the cross-link. The cross-linked peptides were identified through manual interpretation of the raw spectra. To unambiguously assign the cross-linking site, we exhaustively assigned the spectra using in-house written Perl scripts. First, theoretical masses were calculated from the cross-linked peptides, allowing for multiple cross-linking sites and modifications, and then the theoretical masses were matched with mass lists generated by processing the raw spectra with Mascot Distiller 2.0 using an error of 0.1 Da or 100 ppm. Assignments were verified in the raw spectra using isotope patterns and charge states. In some cases, more than one peptide assignment was possible within the experimental error, and then the number of cleavages and supporting ions (e.g., water loss or ammonium loss) was used to select the most likely candidate.

EM reconstruction

G-actin was purified using Superdex-200 column and frozen in liquid nitrogen. Before each experiment, an aliquot of actin was thawed at 4 °C and clarified by centrifugation (100,000*g*, 1 h). Actin (5 μM) was polymerized in 10 mM Tris–HCl buffer, pH 7.8, containing 50 mM KCl, 1 mM $MgCl_2$, 1 mM DTT, and 0.2 mM ATP, for 1.5–2 h. To obtain the filaments decorated with DrABD, we incubated 1–2 μM concentration of F-actin with 10–15 μM concentration of DrABD for 12–15 min at room temperature. An identical procedure was used for decorating actin with the 1–300 drebrin construct. Samples were applied to glow-discharged carbon-coated grids and stained with 2% uranyl acetate. The grids were examined in a Tecnai-12 electron microscope (FEI) under minimal-dose conditions at an accelerating voltage of 80 keV and a nominal magnification of 30,000×.

The SPIDER software package[40] was used for most image processing, but the EMAN package[41] was used to extract filament images from micrographs. A Nikon COOLPIX 8000 scanner was used to digitize micrographs at a raster of 4.16 Å per pixel. The IHRSR method[25] was used to generate an overall reconstruction from 9749 segments (each 416 Å long) of actin filaments decorated with DrABD (Fig. 3b). Comparison of the overall reconstruction with the reconstruction of pure F-actin[17] revealed an additional mass attached to the front and side parts of SD1 and SD2 of actin protomers (see Appendix A for details). To evaluate whether that density was arising from a single drebrin molecule or was rather a superposition of multiple states of binding, we designed a set of models to decompose the additional density into several classes based on the possible location of drebrin on F-actin. The size of the additional mass, along with the quality of the actin portion of the map, was used as a guideline in the sorting process. The position of drebrin in its five modes of binding to F-actin relative to the additional density in the overall reconstruction is shown in Supplemental Fig. 1. A detailed description of the sorting procedures has been published earlier.[26,42]

UCSF Chimera software[43] was used to fit the crystal structure of actin[44] into the experimental maps. Atomic coordinates from crystal structures were converted to density maps, and these were filtered to the resolution of the experimental map and docked manually.

Acknowledgements

This work was supported by the US Public Health Service through grants GM 077190 (to E.R.) and RR 20004 (to J.A.L.), the National Institutes of Health through grant GM081303 (to E.H.E.), and the National Science Foundation through grant MCB 0316269 (to E.R.). We thank Courtney White for helping with isolating drebrin-encoding DNA. We are grateful to Dora Warshaviak for assisting with computational analysis.

Supplementary Data

Supplementary data associated with this article can be found, in the online version, at doi:10.1016/j.jmb.2010.03.039

References

1. Sekino, Y., Kojima, N. & Shirao, T. (2007). Role of actin cytoskeleton in dendritic spine morphogenesis. *Neurochem. Int.* **51**, 92–104.
2. Kojima, N. & Shirao, T. (2007). Synaptic dysfunction and disruption of postsynaptic drebrin–actin complex: a study of neurological disorders accompanied by cognitive deficits. *Neurosci. Res.* **58**, 1–5.
3. Peitsch, W. K., Hofmann, I., Pratzel, S., Grund, C., Kuhn, C., Moll, I *et al.* (2001). Drebrin particles: components in the ensemble of proteins regulating actin dynamics of lamellipodia and filopodia. *Eur. J. Cell Biol.* **80**, 567–579.
4. Peitsch, W. K., Hofmann, I., Endlich, N., Pratzel, S., Kuhn, C., Spring, H. *et al.* (2003). Cell biological and biochemical characterization of drebrin complexes in mesangial cells and podocytes of renal glomeruli. *J. Am. Soc. Nephrol.* **14**, 1452–1463.
5. Grenklo, S., Hillberg, L., Zhao Rathje, L. S., Pinaev, G., Schutt, C. & Lindberg, U. (2008). Tropomyosin assembly intermediates in the control of microfilament system turnover. *Eur. J. Cell Biol.* **87**, 905–920.
6. Ishikawa, R., Hayashi, K., Shirao, T., Xue, Y., Takagi, T., Sasaki, Y. & Kohama, K. (1994). Drebrin, a development-associated brain protein from rat embryo, causes the dissociation of tropomyosin from actin filaments. *J. Biol. Chem.* **269**, 29928–29933.
7. Sasaki, Y., Hayashi, K., Shirao, T., Ishikawa, R. & Kohama, K. (1996). Inhibition by drebrin of the actin-bundling activity of brain fascin, a protein localized in filopodia of growth cones. *J. Neurochem.* **66**, 980–988.
8. Biou, V., Brinkhaus, H., Malenka, R. C. & Matus, A. (2008). Interactions between drebrin and Ras regulate dendritic spine plasticity. *Eur. J. Neurosci.* **27**, 2847–2859.
9. Hayashi, K., Ishikawa, R., Ye, L. H., He, X. L., Takata, K., Kohama, K. & Shirao, T. (1996). Modulatory role of drebrin on the cytoskeleton within dendritic spines in the rat cerebral cortex. *J. Neurosci.* **16**, 7161–7170.
10. Ishikawa, R., Katoh, K., Takahashi, A., Xie, C., Oseki, K., Watanabe, M. *et al.* (2007). Drebrin attenuates the interaction between actin and myosin-V. *Biochem. Biophys. Res. Commun.* **359**, 398–401.
11. Zhao, L., Ma, Q. L., Calon, F., Harris-White, M. E., Yang, F., Lim, G. P. *et al.* (2006). Role of p21-activated kinase pathway defects in the cognitive deficits of Alzheimer disease. *Nat. Neurosci.* **9**, 234–242.
12. Kessels, M. M., Engqvist-Goldstein, A. E. Y. & Drubin, D. G. (2000). Association of mouse actin-binding protein 1 (mAbp1/SH3P7), an Src kinase target, with dynamic regions of the cortical actin cytoskeleton in response to Rac1 activation. *Mol. Biol. Cell*, **11**, 393–412.
13. Xu, W. & Stamnes, M. (2006). The actin-depolymerizing factor homology and charged/helical domains of drebrin and mAbp1 direct membrane binding and localization via distinct interactions with actin. *J. Biol. Chem.* **281**, 11826–11833.
14. Hayashi, K., Ishikawa, R., Kawai-Hirai, R., Takagi, T., Taketomi, A. & Shirao, T. (1999). Domain analysis of the actin-binding and actin-remodeling activities of drebrin. *Exp. Cell Res.* **253**, 673–680.
15. Hayashi, K. & Shirao, T. (1999). Change in the shape of dendritic spines caused by overexpression of drebrin in cultured cortical neurons. *J. Neurosci.* **19**, 3918–3925.
16. Haeckel, A., Ahuja, R., Gundelfinger, E. D., Qualmann, B. & Kessels, M. M. (2008). The actin-binding protein Abp1 controls dendritic spine morphology and is important for spine head and synapse formation. *J. Neurosci.* **28**, 10031–10044.
17. Galkin, V. E., Orlova, A., Lukoyanova, N., Wriggers, W. & Egelman, E. H. (2001). Actin depolymerizing factor stabilizes an existing state of F-actin and can change the tilt of F-actin subunits. *J. Cell Biol.* **153**, 75–86.
18. Reichert, A., Heintz, D., Echner, H., Voelter, W. & Faulstich, H. (1996). Identification of contact sites in the actin–thymosin beta4 complex by distance-dependent thiol cross-linking. *J. Biol. Chem.* **271**, 1301–1308.
19. Kim, E., Miller, C. & Reisler, E. (1996). Polymerization and *in vitro* motility properties of yeast actin: a comparison with rabbit skeletal α-actin. *Biochemistry*, **35**, 16566–16572.

20. Gerson, J. H., Kim, E., Muhlrad, A. & Reisler, E. (2001). Tropomyosin–troponin regulation of actin does not involve subdomain 2 motions. *J. Biol. Chem.* **276**, 18442–18449.
21. Grintsevich, E. E., Benchaar, S. A., Warshaviak, D., Boontheung, P., Halgand, F., Whitelegge, J. P. *et al.* (2008). Mapping the cofilin binding site on yeast G-actin by chemical cross-linking. *J. Mol. Biol.* **377**, 395–409.
22. Cole, C., Barber, J. D. & Barton, G. J. (2008). The Jpred 3 secondary structure prediction server. *Nucleic Acids Res.* **36**, W197–W201.
23. Holmes, K. C., Popp, D., Gebhard, W. & Kabsch, W. (1990). Atomic model of the actin filament. *Nature*, **347**, 44–49.
24. McGough, A., Way, M. & DeRosier, D. (1994). Determination of the alpha-actinin-binding site on actin filaments by cryoelectron microscopy and image analysis. *J. Cell Biol.* **126**, 433–443.
25. Egelman, E. H. (2000). A robust algorithm for the reconstruction of helical filaments using single-particle methods. *Ultramicroscopy*, **85**, 225–234.
26. Galkin, V. E., Orlova, A., VanLoock, M. S., Rybakova, I. N., Ervasti, J. M. & Egelman, E. H. (2002). The utrophin actin-binding domain binds F-actin in two different modes: implications for the spectrin superfamily of proteins. *J. Cell Biol.* **157**, 243–251.
27. Lehman, W., Galinska-Rakoczy, A., Hatch, V., Tobacman, L. S. & Craig, R. (2009). Structural basis for the activation of muscle contraction by troponin and tropomyosin. *J. Mol. Biol.* **388**, 673–681.
28. Bacchiocchi, C., Graceffa, P. & Lehrer, S. S. (2004). Myosin-induced movement of [alpha][alpha], [alpha][beta], and [beta][beta] smooth muscle tropomyosin on actin observed by multisite FRET. *Biophys. J.* **86**, 2295–2307.
29. Lehman, W., Craig, R. & Vibert, P. (1994). Ca^{2+}-induced tropomyosin movement in Limulus thin filaments revealed by three-dimensional reconstruction. *Nature*, **368**, 65–67.
30. Xu, C., Craig, R., Tobacman, L., Horowitz, R. & Lehman, W. (1999). Tropomyosin positions in regulated thin filaments revealed by cryoelectron microscopy. *Biophys. J.* **77**, 985–992.
31. McGough, A., Pope, B., Chiu, W. & Weeds, A. (1997). Cofilin changes the twist of F-actin: implications for actin filament dynamics and cellular function. *J. Cell Biol.* **138**, 771–781.
32. Paavilainen, V. O., Oksanen, E., Goldman, A. & Lappalainen, P. (2008). Structure of the actin-depolymerizing factor homology domain in complex with actin. *J. Cell Biol.* **182**, 51–59.
33. Wyszynski, M., Lin, J., Rao, A., Nigh, E., Beggs, A. H., Craig, A. M. & Sheng, M. (1997). Competitive binding of [alpha]-actinin and calmodulin to the NMDA receptor. *Nature*, **385**, 439–442.
34. Shirao, T. & Sekino, Y. (2001). Clustering and anchoring mechanisms of molecular constituents of postsynaptic scaffolds in dendritic spines. *Neurosci. Res.* **40**, 1–7.
35. Holmes, K. C., Angert, I., Jon Kull, F., Jahn, W. & Schroder, R. R. (2003). Electron cryo-microscopy shows how strong binding of myosin to actin releases nucleotide. *Nature*, **425**, 423–427.
36. Spudich, J. A. & Watt, S. (1971). The regulation of rabbit skeletal muscle contraction: I. Biochemical studies of the interaction of the tropomyosin–troponin complex with actin and the proteolytic fragments of myosin. *J. Biol. Chem.* **246**, 4866–4871.
37. Shevchenko, A., Wilm, M., Vorm, O. & Mann, M. (1996). Mass spectrometric sequencing of proteins from silver-stained polyacrylamide gels. *Anal. Chem.* **68**, 850–858.
38. Ytterberg, A. J., Peltier, J. B. & van Wijk, K. J. (2006). Protein profiling of plastoglobules in chloroplasts and chromoplasts. A surprising site for differential accumulation of metabolic enzymes. *Plant Physiol.* **140**, 984–997.
39. Gobom, J., Nordhoff, E., Mirgorodskaya, E., Ekman, R. & Roepstorff, P. (1999). Sample purification and preparation technique based on nano-scale reversed-phase columns for the sensitive analysis of complex peptide mixtures by matrix-assisted laser desorption/ionization mass spectrometry. *J. Mass Spectrom.* **34**, 105–116.
40. Frank, J., Shimkin, B. & Dowse, H. (1981). Spider—a modular software system for electron image processing. *Ultramicroscopy*, **6**, 343–357.
41. Ludtke, S. J., Baldwin, P. R. & Chiu, W. (1999). EMAN: semiautomated software for high-resolution single-particle reconstructions. *J. Struct. Biol.* **128**, 82–97.
42. Galkin, V. E., Orlova, A., Lukoyanova, N., VanLoock, M. S., Haag, P., Bullard, B. & Egelman, E. H. (2003). The location of ubiquitin in *Lethocerus* arthrin. *J. Mol. Biol.* **325**, 623–628.
43. Pettersen, E. E., Goddard, T. D., Huang, C. C., Couch, G. S., Greenblatt, D. M., Meng, E. C. & Ferrin, T. E. (2004). UCSF Chimera—visualization system for exploratory research and analysis. *J. Comput. Chem.* **25**, 1605–1612.
44. Schutt, C. E., Myslik, J. C., Rozycki, M. D., Goonesekere, N. C. W. & Lindberg, U. (1993). The structure of crystalline profilin–[beta]-actin. *Nature*, **365**, 810–816.